Published in final edited form as:
Eur J Neurosci. 2008 February ; 27(4): 923–936. doi:10.1111/j.1460-9568.2008.06075.x.

Dynamics of Action Potential Backpropagation in Basal Dendrites of Prefrontal Cortical Pyramidal Neurons

Wen-Liang Zhou[1], **Ping Yan**[2], **Joseph P. Wuskell**[2], **Leslie M. Loew**[2], and **Srdjan D. Antic**[1]
[1]Department of Neuroscience, UConn Health Center, Farmington, CT 06030.

[2]Richard D. Berlin Center for Cell Analysis and Modeling, UConn Health Center, Farmington, CT 06030.

Abstract

Basal dendrites of neocortical pyramidal neurons are relatively short and directly attached to the cell body. This allows electrical signals arising in basal dendrites to strongly influence the neuronal output. Likewise, somatic action potentials (APs) should readily propagate back into the basilar dendritic tree to influence synaptic plasticity. Two recent studies, however, determined that sodium APs are severely attenuated in basal dendrites of cortical pyramidal cells, so that they completely fail in distal dendritic segments. Here we used the latest improvements in voltage-sensitive dye imaging technique (Zhou et al., 2007) to study AP backpropagation in basal dendrites of layer 5 pyramidal neurons of the rat prefrontal cortex. With signal-to-noise ratio greater than 15, and minimal temporal averaging (only 4 sweeps) we were able to sample AP waveforms from the very last segments of individual dendritic branches (dendritic tips). We found that in short (<150 μm) and medium range basal dendrites (150 – 200 μm in length) APs backpropagate with modest change in AP half-width or AP rise-time. The lack of substantial change in AP shape and dynamics of rise is inconsistent with the AP failure model. The lack of substantial amplitude boosting of the 3rd AP in the high-frequency burst, also suggests that in short and medium range basal dendrites backpropagating APs are not severely attenuated. Our results show that the AP failure concept does not apply in all basal dendrites of the rat prefrontal cortex. The majority of synaptic contacts in the basilar dendritic tree, actually, receive significant AP-associated electrical and calcium transients.

Keywords

prefrontal cortex; pyramidal neurons; basal dendrites; action potential; backpropagation; voltage-sensitive dyes

Introduction

Basal dendrites dominate the dendritic tree of cortical pyramidal neurons and seem to have an important role in synaptic integration (Enoki *et al.*, 2004; Polsky *et al.*, 2004; Araya *et al.*, 2006). Basal dendrites are directly attached to the cell body, and as such are capable of delivering large amplitudes of synaptically-evoked depolarizing currents (Schiller *et al.*, 2000; Oakley *et al.*, 2001) and strongly influencing the neuronal action potential output (London *et al.*, 2002; Milojkovic *et al.*, 2005a). Basal dendrites receive a substantial fraction of all synaptic contacts impinging on the pyramidal dendritic tree (Larkman, 1991). In cortical pyramidal cells numerous basal afferents originate from pyramidal neurons in the same vertical

Corresponding author with complete address, including an email address, Srdjan D. Antic, Dept. Neuroscience, L-4000, UConn Health Center, 263 Farmington Ave., Farmington, CT 06030-3401, E-mail: antic@neuron.uchc.edu, Tel: 860-679-8468, Fax: 860-679-8766.

microcolumn (Burkhalter, 1989; Staiger *et al.*, 2000; Feldmeyer *et al.*, 2002; Lubke *et al.*, 2003), as well as from pyramidal neurons in the same horizontal lamina (Levitt *et al.*, 1993; Markram, 1997; Thomson & Bannister, 2003; Morishima & Kawaguchi, 2006). In the prefrontal cortex, multiple synaptic contacts between neighboring L5 pyramidal neurons are made exclusively onto basal dendrites (Wang *et al.*, 2006). This dense reciprocal excitatory arrangement between nearby cortical pyramidal cells provides structural support for strong recurrent excitation, which is thought to comprise the cellular substrate of persistent activity - working memory (Goldman-Rakic, 1995). Higher cognitive functions, such as learning and memory, depend on synaptic plasticity, which is a Ca^{2+}-mediated cellular process (Lisman *et al.*, 1997; Linden, 1999; Zucker, 1999). Sodium action potentials (APs) propagate from the axon-soma compartment into dendritic branches to open voltage-gated calcium channels, NMDA receptor-channels, and bring Ca^{2+} ions to synaptic contacts (Jaffe *et al.*, 1992; Magee & Johnston, 1997; Markram *et al.*, 1997). At present it is not known how successfully APs invade basal dendrites of the prefrontal cortical cells.

The first experimental measurement of AP backpropagation in the basal dendrites of cortical pyramidal neurons was performed in the somatosensory cortex at room temperature (Antic, 2003). Based on multi-site voltage-sensitive dye (VSD) recordings and multicompartmental modeling, this study led to a conclusion that basal dendrites impose modest amplitude and shape modulation on backpropagating action potentials. Using the same technique, and in the same cortical area (somatosensory cortex), but at the physiological temperature (35±1°C), Kampa and Stuart (2006) found that APs were significantly attenuated in distal segments of basal branches. According to their model, amplitude reduction is so severe that in the dendritic region between 150 and 250 μm from the soma the amplitude of backpropagating AP (b-AP) is only ¼ of that measured in the cell body (their Fig. 7B2). Nevian et al., 2007 attained patch clamp recordings from the proximal 140 μm of basal dendrites and concluded that proximal recordings strongly support the Kampa and Stuart (2006) AP-failure model.

Here we used fast optical imaging with internally applied voltage-sensitive dyes to study the membrane potential changes in remote dendritic regions (Antic *et al.*, 1999). We investigated the dynamics of AP backpropagation in basal dendrites of prefrontal pyramidal cell at physiological temperature (34°C), and found that the AP backpropagation model characterized with severe amplitude reduction and dramatic increase in AP half-width (Kampa & Stuart, 2006) does not apply in short (<150 μm) and medium range (150–200 μm) dendritic branches. We were able to sample membrane potential transients from distal dendritic tips (the last segment on a dendrite) using recent improvements in dye sensitivity and experimental design (Zhou et al., 2007). Voltage recordings from the very last dendritic segment have never been achieved before. Consequently, little is know about the nature of electrical transients in this terminal dendritic segment, and how a backpropagating AP interacts with local synaptic contacts in this particular segment. In addition, by sampling the AP time course from the tip of the dendrite we eliminated any uncertainty of what the signal might look like distally from the recording site. This achievement is especially useful for constraining the realistic biophysical models designed to study AP backpropagation in the basilar dendritic tree. The technical improvements also allowed us to reduce the number of sweeps used for temporal averaging from 100 (Kampa & Stuart, 2006) to just 4. In this way we minimized the distortions, which AP temporal jitter and trial-to-trial variability in AP amplitude and half-width (during extensive averaging sessions) may impose on the time course of the fast electrical transient. We often found that AP peak latency is less than 1 millisecond, even in the most distal dendritic segments of short and medium range basal branches. Second, the half-width of the b-AP remains relatively unchanged along the entire dendritic branch, all the way to the distal tip. Third, the same was true for the rise time of b-APs. The rise-time of the AP signal at the very end of the dendritic branch (distal dendritic tip) is almost the same as in the most proximal dendritic segment, which is inconsistent with significant cable filtering of APs. Finally, the

frequency-induced boosting of the 3rd AP in the triplet of action potentials, which was used as a crucial evidence for AP failure in Kampa and Stuart (2006) paper, was negligible in a large part of the basilar dendritic tree. More precisely, the relative amplitude increase for the 3rd AP over the 1st AP in a high-frequency AP burst was small (less than 25% on average); approximately 4 times smaller than the value recently reported in basal dendrites of cortical neurons (Kampa & Stuart, 2006). This was true in the proximal 130 μm, as well as in the dendritic segments more than 130 μm away from the soma. Taken together, our data indicate that in the majority of short and medium range basilar branches of prefrontal cortical pyramidal neurons the backpropagating APs are not severely attenuated. Interactions between backpropagating APs and synaptic contacts located on basal dendrites of pyramidal neurons have recently triggered much interest among neuroscientists (Koester & Sakmann, 1998; Gordon *et al.*, 2006; Kampa *et al.*, 2006; Nevian & Sakmann, 2006; Sjostrom & Hausser, 2006). Information presented in this manuscript is expected to improve our understanding of the physiological properties of basal dendrites in the prefrontal cortex, and their potential role in spike-dependent synaptic plasticity (Linden, 1999; Dan & Poo, 2004; Holthoff *et al.*, 2006).

Material and Methods

Brain slice and electrophysiology

Sprague Dawley rats (P21 – 42) were anesthetized with isoflurane, decapitated, and the brains were removed with the head immersed in ice-cold, artificial cerebrospinal fluid (ACSF), according to an animal protocol approved by the Center for Laboratory Animal Care, University of Connecticut. ACSF contained (in mM) 125 NaCl, 26 $NaHCO_3$, 10 glucose, 2.3 KCl, 1.26 KH_2PO_4, 2 $CaCl_2$ and 1 $MgSO_4$, pH 7.4. Coronal slices (300 μm) were cut from frontal lobes anterior to genu corpus callosum. Whole-cell recordings were made from visually identified layer 5 pyramidal neurons, on the medial part of the slice, as depicted in (Gulledge & Jaffe, 1998) (their figure 1). Intracellular solution contained (in mM) 135 K-gluconate, 2 $MgCl_2$, 3 Na_2-ATP, 10 Na_2-phosphocreatine, 0.3 Na_2-GTP and 10 Hepes (pH 7.3, adjusted with KOH). Electrical signals were amplified with Multiclamp 700A and digitized with two input boards: (1) Digidata Series 1322A (Molecular Devices, Union City, CA) at 5 kHz, and (2) Neuroplex (RedShirtImaging, Decatur, GA) at 2.7 kHz sampling rate. In experiments presented in Fig. 9 whole-cell signals were sampled at 10 kHz. Only cells with a membrane potential more hyperpolarized than −50 mV, and action potential amplitudes exceeding 80 mV (measured from the base line) were included in this study. All experiments were performed on layer 5 pyramidal cells at 34°C. Triplets of action potentials (Fig. 6) were evoked with three depolarizing current steps injected into the cell body (intensity 1 – 1.5 nA, duration 1.5 – 2 ms, frequency 125 Hz).

In the experiments shown in Fig. 9 dual somatic patch-clamp recordings were performed using two identical head stages (CV-07). Both channels were amplified using the same amplifier (Multiclamp 700A) and digitized under identical conditions using the same A-D board (Digidata 1322A Series, Molecular Devices, Union City, CA). Pipette capacitance neutralizations and series resistance compensation were performed on both channels prior to each data acquisition sweep, using current injections delivered through both pipettes interchangeably (Fig. 9B, lower traces). Electronic compensation of pipette capacitance was performed using pipette capacitance neutralization command in Multiclamp Commander. Neutralization was increased as far as possible without provoking oscillations – usually between 8–9 pF. Figure 9C depicts the effect of 9 different neutralization values 1 – 9 pF on the amplitude and waveform of the fast AP signal. Following each 1-pF-step-increase the series resistance was compensated using the bridge balance and recordings were acquired and stored

on the disk. For plotting in Fig. 9D only the best sweep (highest possible value for capacitance neutralization) was used.

Dye Injections

The dye injection protocol was previously described in (Antic, 2003). Briefly, neurons were filled through whole-cell recording pipettes with one of the following styryl voltage-sensitive dyes JPW3028, JPW4090, JPW3080 or PY1286, dissolved in standard K-gluconate based intracellular solution. Red dye, JPW3028, was stored in final solution at +4°C for up to a month. Blue dyes, JPW4090, JPW3080 or PY1286 were stored in ethanol stock solution at −20°C. On the day of the recording blue dyes were dissolved in intracellular solution. Loading pipettes were filled with two varieties of the same intracelslular solution; one with and one without the dye. Dye-free solution was occupying the very tip of the pipette, while the back of the pipette lumen was microloaded with dye-rich solution (400 – 800 μM). The purpose of dye-free solution in the tip of the patch pipette was to prevent dye-leak during the maneuver through brain slice tissue. Both red and blue VSDs are lipophilic and bind indiscriminately and irreversibly to all membranes around the neuron of interest. Even a small amount of dye that leaks out of the pipette during the formation of the gigaohm seal can generate strong fluorescent background. Fluorescent light emanating from surrounding tissue has a devastating effect on dendritic optical signals. Elimination of the background fluorescence is critical for dendritic voltage imaging. How much dye-free solution one should put in the tip depends on time period between the submersion of the patch pipette into the recording chamber and formation of the gigaohm seal. The faster one can perform this maneuver the less dye-free solution she needs to achieve optimal staining. VSD were injected at room temperature for 25–60 minutes. The filling pipette was carefully pulled out (outside-out patch) and brain slices were left to incubate for 20–120 minutes at room temperature. Just before optical recordings the cells were re-patched with dye-free pipette at physiological temperature (34°C).

Dendritic voltage imaging

Voltage-sensitive dye imaging was performed on a Zeiss Axioskope 2FS microscope equipped with NeuroCCD camera (RedShirtImaging). We used Zeiss 40X objective IR-Achroplan 0.80 NA. In the place of the arc lamp (normally used for epi-illumination), we inserted a Φ200 μm fiber optic guide with a collimator. Laser beam was focused on the other side of the fiber optic guide using a microscope objective lens. This arrangement produced a motionless spot of laser light (25 – 50 μm in diameter) at the object plane (Fig. 1A, C). A region of interest (ROI) was brought into the laser spot using X-Y microscope platform. The laser beam was interrupted by an electro-programmable shutter (Uniblitz, Vincent Associates, Rochester, NY). Attention was made to limit the exposure time during the recording and positioning of the neuron. Focusing and positioning was done at lower light level intensities – regulated by neutral density filters inserted in the epi-illumination path. In the course of this experimental study we used three different laser light sources, Cobolt Samba (150 mW), HeNe (20 mW), and laser diode (80 mW), with peak excitations centered at 532, 633, and 658 nm, respectively. Laser beams were directed onto the preparation with the help of Zeiss epi-illumination filter cubes. For 532 nm laser epi-illumination we used a filter cube with a following set of optical filters: exciter 520 ± 45 nm; dichroic 570 nm; emission >610 nm. For 633 nm laser epi-illumination we used exciter 640/30 nm, dichroic 660 nm and emission 665 nm long-pass. Having an excitation filter in the cube did not make any difference in experiments with laser lines 532 nm and 633 nm, so we simply left the excitation filters in place. For 658 nm laser epi-illumination we used 700 nm dichroic, and 720 nm long-pass emission filter (no exciter).

Optical signals were recorded with 80 × 80 pixels (Fig. 1C) at a 2.7 kHz frame rate, stored, and then temporally filtered (off-line) with digital Gaussian low-pass filter (1050 Hz cut-off), and Butterworth high-pass (4.5 Hz), unless otherwise specified. To correct for photobleaching

artifact the trace without stimulus was recorded at the end of experiment and subtracted from physiological recordings. The term ROI (region of interest) we use to mark selected neuronal compartments, where membrane potential transients were measured either optically (voltage-sensitive dyes) or electrically (whole-cell). To improve signal-to-noise ratio several pixels (3 – 8 pixels) were selected inside the region of interest and spatially averaged, unless otherwise specified. For temporal averaging we used a spike-triggered routine available in Neuroplex (RedShirtImaging). The number of sweeps used for temporal averaging did not exceed 9. An example of the optical trace obtained using spatial (8 pixels) and temporal (4 sweeps) is shown in Fig. 1D. With 40X magnification lens, used in this study, each pixel covers 4.8 × 4.8 μm in the object field (Fig. 1C). After the experiment, fluorescent images were captured with IR-1000 Dage CCD camera (Fig. 1A, B). In order to obtain whole-field photographs of the dendritic tree, brain slices were removed from the recording chamber and mounted on a microscope slide in water-based mounting medium (Biomeda, Foster City, Ca). Mounted microscope slides were transferred to Zeiss Axiovert200M imaging station where photographs were taken with AxioVision LE system using 20x dry and 40x oil immersion objectives (Fig. 4A, C).

Dendritic calcium imaging

For dendritic calcium imaging we used the same optical setup described above except instead of lasers we employed 150 W arc lamp (Opti-Quip, Highland Mills, NY). Ca-sensitive dye Ca-Green-1 [200 μM] was mixed with Alexa Fluor 594 [60–80 μM] and injected through 7 MΩ patch pipettes for at least 35 min before recordings were made. As previously described for voltage-sensitive dyes here too a dye free solution was used in the tip of the patch pipette to prevent leakage of fluorescent molecules and contamination of the brain slice (background fluorescence). For Ca^{2+} imaging we used a filter cube loaded with exciter 480±30 nm), dichroic 515 nm, and emitter 530 nm long-pass. Ca^{2+} signals were sampled at 200 Hz frame rate (5 ms sampling interval) using NeuroCCD camera.

Data analysis

Optical and electrical measurements were analyzed using the software Neuroplex (RedShirtImaging) and Clampfit 9.1 (Axon Instruments). Graph plotting was done in Excel. Amino-naphthyl styryl dyes JPW3028, JPW4090, JPW3080 and PY1286 used in this study have identical optical response to membrane potential change (Zhou *et al.*, 2007), so we grouped data points obtained with 4 indicators. Although, voltage-sensitive dyes accurately report the time course of the membrane potential change, and show linear amplitude response in the biologically relevant range −100 to +100 mV (Ross *et al.*, 1977), when applied intracellularly they cannot report the absolute amplitude (in mV) of the electrical transient. This issue has been thoroughly discussed in the literature (Antic *et al.*, 1999; Antic, 2003). All amplitude measurements in this study are presented in relative terms; as percentage change relative to first AP in the burst. For example, in Fig. 6 amplitudes of 2^{nd} and 3^{rd} action potentials were measured from the base line and expressed as percentage of the 1^{st} AP amplitude. AP rise-time was defined as time interval required for optical signal to rise from 10% to 90% of its peak amplitude. AP half-width was defined as duration of signal at 50% amplitude. AP peak latency was defined as time interval between the peaks of somatic and dendritic spikes. AP rise-time, AP half-with and AP peak latency were measured using programs written in MATLAB (MathWorks, Bethesda, MD) and LabView (National Instruments, Austin, TX) by Corey Acker (UConn Health Center) and Matt Wachowiak (Boston University). Prior to measurements AP waveforms were interpolated (over-sampled to 27 kHz) as described in Antic (2003). All error bars in figures were calculated as the mean ± s.e.m., and data in the text are reported as means ± s.d. N = number of dendrites; n = number of neurons.

Results

Increase in AP half-width suggests AP propagation failure

Voltage-sensitive dyes were used to record AP waveforms from the most distal segments of short (<150 μm) and medium range (150–200 μm) basal branches (Fig. 2A). Simultaneously with optical imaging, AP waveforms were recorded electrically from the cell body. In the example shown in Fig. 2, AP waveforms were analyzed in 5 basal branches belonging to the same neuron. In 4 out 5 branches the half-width of the single backpropagating AP was similar to that measured in the cell body (B2 – E2). During high frequency AP firing (train of 3 APs at 80 Hz) the amplitudes of three dendritic spikes were relatively uniform in the most distal segments of 4 basal branches (B3 – E3). However, in 1 out of 5 dendrites the AP half-width was approximately 2 times greater than that obtained in the soma (Fig. 2F2, ROI 5), and the amplitude of the 1st spike in the triplet (Fig. 2F3, arrow) was >2 times smaller than the 2nd and 3rd spike. This was observed in four PFC layer V neurons at 5 recordings sites (5 dendrites). In these five recordings the amplitude of the second dendritic spike was on average 1.70 ± 0.12 (ave. ± s.d.) of the first spike amplitude. The amplitude of the third spike was 1.92 ± 0.29 greater than the amplitude of the first spike (N=5 dendrites). Paired T-test showed that differences in amplitude between the 2nd and 3rd spikes compare to 1st were highly significant ($p<0.001$ and $p<0.001$, respectively). Since temporal averaging (3–4 sweeps) was used to obtain these data, it should be noted that this result might be the effect of averaging. For example, intermittent failures of the 1st and 2nd spike could produce amplitude differences in the average trace. However, this was not the case. We saved individual sweeps used for averaging (Suppl. Fig. 1; Sweep 1–4). The amplitude of the 1st spike was drastically smaller than subsequent spikes in all recording sweeps without exceptions (4 neurons; 5 dendrites, 19 recordings sweeps). A 2–3 fold boosting of dendritic AP amplitude during high frequency firing (Fig. 2F3) is a strong indicator of AP propagation failure (discussed in Kampa and Stuart, 2006). The results presented in Fig. 2 and Suppl. Fig. 1 indicate that **(1)** AP propagation failures occur in some basal dendrites of prefrontal layer 5 pyramidal neurons; **(2)** An increase in AP half-width (Fig. 2G) is an important sign of AP propagation failure; **(3)** A large boosting of the 2nd and 3rd spike amplitude is a sign of 1st AP failure; and **(4)** Our experimental design based on internally applied voltage-sensitive dyes and laser spot illumination can reliably detect AP propagation failures in thin basal dendrites of pyramidal neurons.

AP half-width and AP peak latency

Using the voltage-sensitive dye technique described in Fig. 1 we analyzed AP dynamics in the most distal segments (terminals) of 46 basal dendrites of 21 layer 5 pyramidal neurons in the rat prefrontal cortex. Due to insufficient sensitivity of the voltage-sensitive dyes and their slow diffusion through the dendritic tree we were not able to obtain recordings from the terminals of basal branches whose length exceeded 250 μm. In the present data set an average length of basilar dendritic branches was 173 ± 32 μm (N=46, full range 120 – 245 μm). An average AP duration measured at half amplitude (half-width) in the soma was 1.01 ± 0.15 ms, while at the dendritic terminal it was 1.20 ± 0.15 ms (N = 46). We calculated AP half-width ratio between the dendritic tip and soma of the same cell, and found that the half-width of dendritic AP was on average 121 ± 18 % (N = 46) of the somatic AP half-width (Fig. 3C).

The AP peak latency in the distal dendritic tip varied depending on the length of the basal dendrite. Shorter branches (less than 150 μm) typically backpropagate APs to the very end of their structure, in a sub-millisecond time window (Fig. 3D). Longer basal branches required a little bit longer time to reach the terminal segment. In 21 neurons (46 measurements from dendritic tips only, Fig. 3A) the AP peak latency did not exceed 1.37 ms. The majority of measurements (17 out of 26) performed in distal dendritic tips, between 170 and 245 μm from the soma, showed AP peak latencies smaller than 1.0 ms (Fig. 3D, below horizontal line). Small

changes in AP shape (Fig. 3BC), combined with a sub-millisecond propagation time window (Fig. 3D), suggest that backpropagating APs are not severely attenuated in the short (<150 nm) and medium range (150–200 μm) basal dendrites of prefrontal cortical neurons.

Trains of APs

It is now well established that trains of sodium action potentials backpropagate along apical dendrites in a frequency and spike-order dependent manner. For example, at 20–50 Hz AP firing rate the later spikes in the train undergo a stronger degree of amplitude attenuation than the first spike in the train (Spruston *et al.*, 1995; Stuart *et al.*, 1997; Larkum *et al.*, 2001). We tested this scenario in basal dendrites of prefrontal cortical neurons using intracellularly applied voltage-sensitive dyes (Fig. 4A, C) and laser spot illumination (4B, D). Trains of APs composed of 10 spikes (inter-spike interval 20 ms) were evoked by 10 brief depolarizing pulses injected into the cell body (4E, 0). Trains of backpropagating APs were recorded from 7 dendritic sites (4E, ROI 1 and 2) in 3 pyramidal neurons at an average distance from the cell body of 127 + 22 μm. At 50 Hz AP firing rate we found no evidence for frequency and temporal-order-dependent AP amplitude attenuation (Fig. 4F). That is to say that APs 2 – 10 did not have statistically different amplitudes from the 1st spike in the train ($p>0.05$).

The AP frequency used in the previous experiment (50 Hz) is perhaps too low to cause frequency dependent amplitude changes of b-APs in basal dendrites. Kampa and Stuart (2006) discovered that a high frequency AP bursts can recruit voltage-gated sodium and voltage-gated Ca^{2+} channels in the basal dendrite and produce dramatic boosting of the 3rd AP in the train. Their results indicate that the peak amplitude of the third AP in the burst was on average two-fold greater (gain of ~ 100%) than the first AP. This was the crucial evidence that single APs undergo significant attenuation at distal basal dendritic locations. Previous studies on pyramidal neurons in the rat somatosensory cortex have also determined that 100 Hz is the critical frequency for activation of the dendritic voltage-gated Ca^{2+} channels (Larkum 1999). We triggered triplets of sodium APs at 125 Hz and measured voltage-sensitive dye signals from basal dendrites of prefrontal cortical L5 neurons (Fig. 5B). We are aware that such a high frequency of AP firing is not characteristic for the mammalian prefrontal cortex (PFC). PFC pyramidal neurons in awake behaving rats and non-human primates typically occur in the range 0.5 – 40 Hz (Williams & Goldman-Rakic, 1995; Chafee & Goldman-Rakic, 1998; Chang *et al.*, 2000; Ramus & Eichenbaum, 2000; Homayoun & Moghaddam, 2006). In the present study a 125 Hz AP firing rate was only used for testing the biophysical properties of individual pyramidal cells. Using this stimulation paradigm (125 Hz AP triplets), we carried out optical measurements from multiple sites on individual dendritic branches. Measurements were performed sequentially; one region of interest (ROI) at the time, in subsequent recording sweeps (Fig. 5, Fig. 1–Fig. 5). We were able to achieve excellent signal-to-noise ratio using as few as 4 trials for temporal averaging per ROI. Having a good signal quality allowed us to monitor the consistency of dendritic voltage response across individual sweeps used for averaging. For example, Supplemental Fig. 2 reveals 4 individual sweeps (sweep 1 – 4), which were used to produce the final trace (ave. of 4) at the distal dendritic tip 185 μm away from the cell body (Fig. 5B, ROI 5). In each trace (sweep 1 – 4) the amplitudes of three dendritic spikes were roughly the same, thus providing evidence that the average trace (ave. of 4) is a faithful representation of the event under study. More importantly, the systematic monitoring of individual sweeps provides evidence that AP backpropagation in this part of the dendritic tree, and under the current *in vitro* conditions, is robust and reliable process. In other words, intermittent spike propagation failures or changes in shape or amplitude, from sweep to sweep, were not observed.

Numerical analysis of 125 Hz AP triplets showed that the amplitude of the 3rd AP at proximal dendritic sites (less than 130 μm away from the soma) was on average 105.5 ± 1.2 % of the

1st AP (Fig. 6C). Recordings were performed at 31 dendritic recording sites less than 130 μm away from the soma (n=16 neurons, N=31 recording sites, Average distance from the soma = 94 ± 27 μm). Similar results were obtained at distal dendritic sites, more than 130 μm away from the soma. At distal dendritic segments (>130 μm) the amplitude of the 3rd AP was on average 115.4 ± 15.9% of the amplitude of the 1st AP (Fig. 6D, n=16). Recordings were performed at 29 dendritic recording sites more than 130 μm away from the soma (n=16 neurons, N=29 recording sites, Average distance from the soma = 175 ± 37 μm). A small increase in AP amplitude was also detected in the case of a 2nd AP; at both proximal (<130 μm; 104.8 +0.9%, n=16) and distal dendritic sites (>130 μm; 106.5+1.1%; n=16). AP triplets in the somatic whole-cell recordings were relatively uniform in amplitude (Fig. 6CD, Soma). Namely, the relative amplitude of the 3rd somatic spike was 96.9% (for data set <130 μm) and 95.7% (for data set >130 μm) of the 1st somatic spike. In summary, while somatic action potentials show a small (~5%) decrease in AP amplitude with temporal order (Fig. 6CD, Soma, 3rd), the dendritic b-APs undergo a small (~15%) increase in amplitude (Fig. 6CD, Dend. 3rd).

In contrast to AP amplitude, the AP half-widths in dendritic recording sites showed a notable >60% growth with the temporal order of the spike (Fig. 6EF, Dend., 3rd AP). The growth in AP half-width among subsequent spikes was not a unique feature of dendritic recordings (compare 6A and 6B). A nearly identical (~60%) relative increase in 3rd AP half-width was observed in the somatic whole-cell recordings of all neurons in both data sets (Fig. 6EF, Soma). More precisely, the half-width of the 2nd and 3rd AP in the somatic triplet (whole-cell recordings) was 135 ± 13% and 163 ± 24% of the 1st spike for <130 μm data set (N=31); 138 ± 16% and 164 ± 21%, for >130 μm data set, respectively (N=29). Half-widths of 2nd somatic and 2nd dendritic AP were not statistically different ($p>0.05$). Also, the half-widths of 3rd somatic and 3rd dendritic AP were not statistically different ($p>0.05$) for both data sets. In fact, there was a strong correlation between corresponding somatic and dendritic AP wave-forms (Coefficient Correlation$_{2nd}$ = 0.49; CC_{3rd} = 0.62 for <130 μm (N=31), and CC_{2nd} = 0.74, CC_{3rd} = 0.60 for >130 μm data set (N=29)). These data suggest that dendritic cable filtering was not responsible for large changes in AP half-width observed for 2nd and 3rd spike in the 125 Hz triplet. The dendritic membrane did not impose changes on relative AP half-widths within the burst, and did not introduce any significant changes in the AP waveforms that were not already present in the cell body.

We grouped 115 recordings obtained in 37 neurons and plotted three characteristic biophysical parameters (AP half-width, AP peak-latency, and AP rise-time) versus distance from the cell body (Fig. 7). Five recordings showing an obvious AP failure (Fig. 2F3, arrow) were excluded from the graphs (Fig. 7). The data set in Figure 7 includes recordings of single action potentials and recordings of the first AP in the triplet, at all distances, including the most distal dendritic tips. In this data set the absolute half-width of backpropagating action potentials (in ms) showed minimal change along the length of short basilar branches (Fig. 7A). We then divided the half-width of the dendritic spike with the half-width of the corresponding somatic AP and plotted these values in panel B. This type of analysis was able to detect a small systematic relative increase in AP half-width with distance from the cell body (positive slope of the linear fit in Fig. 7B). We measured the time period which is required for an AP to rise from 10 to 90% of its peak amplitude (rise-time). To our surprise, the plot of the AP rise-time showed a minimal increase vs. distance from the cell body. The slope of the linear fit was 1×10^{-4} (Fig. 7D). The only biophysical parameter that showed a clear non-uniform distribution along basal dendrites was the AP peak latency (Fig. 7C). The peak of a dendritic AP invariably occurred after the peak of the somatic spike. This time interval increased as we moved our recording site (ROI) along the contours of the basilar dendritic branches (Fig. 5, ROI 1–5). A great majority of data points (128 out of 137) fell below 1 ms (Fig. 7C). AP peak latencies were used to calculate AP

propagation velocity in basal dendrites of prefrontal cortical layer 5 pyramidal neurons. A linear fit through data points (Fig. 7C) had a slope of 0.39 m/s (R^2=0.61).

AP-associated Ca^{2+} transients in the tips of basal dendrites

As a result of severe attenuation along basal branches, the amplitudes of b-APs might be too small to depolarize distal dendritic segments and open voltage-gated Ca^{2+} channels (VGCC). Indeed, in layer 5 pyramidal neurons of the rat somatosensory cortex single APs fail to evoke Ca^{2+} transient in basilar dendrites 210 μm from the cell body (Kampa and Stuart, 2006; their fig. 1D). We investigated this issue in the rat prefrontal cortex using calcium-sensitive dye Ca-Green-1. We focused on the very last segments of basal branches – dendritic tips. In 4 neurons we found 4 dendritic tips (162 – 265 μm from the soma) where single backpropagating APs did not generate any measurable Ca^{2+} signal (data not shown). However, in 23 cells we recorded from the very last segment of multiple basal dendrites (Fig. 8A, ROIs 2, 3, 4 and 6) and obtained clear Ca^{2+} transients associated with the first spike in the train (Fig. 8B–D, arrows). In this data set the average distance between the dendritic tip and cell body was 203 ± 32 μm (N=38, full range 131 – 265 μm). At each recording site (N = 38 basal dendritic tips; n = 23 neurons) strong and sharp Ca^{2+} transients were invariably detected during triplets of APs. Each AP in the high frequency train triggered a distinct Ca^{2+} transient. Most importantly, the very first AP in the train was regularly producing detectable Ca^{2+} signals in terminal dendritic segments (Fig. 8B–D, arrows). The same was true for a single AP (Suppl. Fig. 3D). These results indicate that in many cases the amplitude of the backpropagating AP is large enough to substantially depolarize the tips of basal dendrites and cause influx of Ca^{2+}. The shape of the dendritic Ca^{2+} transient in the terminal segment, characterized by fast rise, sharp peak and fast exponential decay (Fig. 8B–D; Suppl. Fig. 3D, ROIs 1–3) is inconsistent with severe action potential failure in these dendritic branches.

Discussion

Sodium action potentials backpropagate into the basal dendrites of neocortical pyramidal neurons and influence the plasticity of numerous synaptic contacts impinging in this part of the dendritic tree (Kampa *et al.*, 2006; Nevian & Sakmann, 2006; Sjostrom & Hausser, 2006). Given the importance of the prefrontal cortex (PFC) and the fact that basal dendrites of PFC cortical neurons contain greater number of synaptic contacts than basal dendrites in any other cortical area (Elston *et al.*, 2001), it is necessary to determine the efficacy of AP backpropagation in this brain region. Experimental analysis of AP waveform in the most distal (terminal) segment of any dendrite in the CNS has never been achieved before due to technical limitations associated with recordings from processes with submicron diameter. Using intracellular voltage-sensitive dyes and laser illumination (Zhou et al., 2007) we analyzed the time course of a backpropagating action potential in the terminal segments of PFC basal branches (Fig. 1 and Fig. 2). AP associated signals were obtained from dendritic tips with excellent signal-to-noise ratio - greater than 15. Less than 9 sweeps, and in many cases just 4 sweeps (Fig. 1, Fig. 2, Fig. 4, and Fig. 5), were averaged to achieve this quality of optical records. The VSD recording technique does not permit absolute measurements of the AP amplitude in terms of mV (Antic, 2003). No conclusions in the present study have been made based on the comparison of signal amplitude between two regions of the same cell. In the present data analysis, AP amplitudes were expressed in relative terms only. For example, the amplitude of the 3rd spike in the burst was divided by the amplitude of the 1st spike and expressed as percentage (Fig. 4F and Fig. 6C–F). Because the sensitivity of the voltage-sensitive dye measurement is unlikely to change within 100 ms, which is the duration of one recording episode (sweep), it is appropriate to compare subsequent transients within the same sweep (Fig. 6B). This type of analysis was first used in Antic (2003) (his Fig. 9) and later in Kampa and Stuart (2006).

Based on the study by Kampa and Stuart (2006) there are five signs of AP failure in basal dendrites: (1) a dramatic (200 – 300 %) increase in dendritic AP half-width compare to AP in the soma; (2) exponential increase in AP peak latency, reaching 2 ms in the most remote segments; (3) significant increase in AP rise-time with distance; (4) amplitude boosting of the 3rd AP in the high-frequency burst; and (5) failure of single APs to trigger Ca^{2+} transients in distal dendritic segments (Kampa & Stuart, 2006). Our measurements show that sodium APs backpropagate all the way to the distal dendritic tips of short and medium range basal dendrites with moderate change in shape (Fig. 3C). This finding, together with sub-millisecond AP latency (Fig. 3D), relatively uniform AP rise time (Fig. 7D), lack of substantial AP amplitude boosting (Fig. 6), and strong and sharp Ca^{2+} transients in dendritic terminals (Fig. 8; Suppl. Fig. 3), is inconsistent with the complete failure of AP propagation, previously described in the long basal dendrites of the rat somatosensory cortex (Kampa & Stuart, 2006).

Several possible reasons may explain the differences between our data and the Kampa and Stuart (2006) results. In the present study, we used less than 9 sweeps for temporal averaging, while Kampa and Stuart (2006) used up to 100 sweeps to obtain AP associated optical signals from basal dendrites. Extensive averaging is necessary when a signal is very small and buried in the noise. In the case of action potential imaging, extensive averaging carries two serious risks. First, a small jitter in the timing of APs, as well as possible changes in AP amplitude and shape from trial to trial, produce an averaged trace that is distorted in time domain. Second, repeated illumination of the same cellular compartment may cause photodynamic damage, which severely impairs the membrane physiology and causes changes in the electrical signal. The first sign of VSD-induced phototoxicity is actually the broadening of a sodium AP (Antic et al. 1999).

Filtering of optical signals is another factor that may explain the difference between Kampa and Stuart (2006) and our data. The 500 Hz cutoff frequency of the low pass filter used by Kampa and Stuart (2006) strongly affects the amplitude and shape of the first AP in the train of spikes. In cortical pyramidal neurons, the first AP in the train has the shortest duration (half-width) as depicted in Fig. 1, Fig. 2 and Fig. 6. The 1st AP, being the fastest transient, is more affected by low pass filtering than the slowest transient in the AP triplet (3rd AP). We filtered the dendritic optical signals and found that low pass filtering at 500 Hz cutoff produces a severe distortion in the relative AP amplitude. Before filtering, all 3 APs have uniform amplitudes (Fig. 6B). After filtering (low-pass filter 500 HZ cutoff), the amplitude of the 3rd AP is notably greater than the amplitude of the 1st AP (Fig. 6H). To make sure that the problem with low pass filtering is not inherent to our optical recordings, we performed the same exercise using whole-cell records obtained from the soma. As previously seen for dendritic records, a perfectly uniform set of 3 somatic AP (Fig. 6A) invariably turned into a non-uniform triplet (3rd spike is “boosted”) after application of a low pass filter with 500 Hz cutoff (Fig. 6G).

Recently Nevian et al., 2007 used extremely small patch pipettes (electrode resistance 40 – 50 MΩ) to patch onto basal dendrites in the rat somatosensory cortex. Because of high electrode resistance, the access resistance in their whole-cell dendritic recordings reached the value of 200 MΩ. Nevertheless, Nevian et al. (2007) concluded that sodium APs are significantly attenuated in the basal dendrites, thus providing strong support for the Kampa and Stuart (2006) AP-failure model. In order to determine how small patch pipettes affect membrane potential transients, we recorded from the cell body of a layer 5 pyramidal neuron using two patch-clamp pipettes (Fig. 9A, Inset). When pipettes P1 and P2 were of regular size (electrode resistance 5 – 8 MΩ) the amplitude of AP signal in two channels was identical (Fig. 9A, dashed line). However, when one pipette (P1) was a regular-size patch pipette for whole-cell somatic recordings (6 MΩ) and the second pipette (P2) had high resistance in the bath (44 MΩ) the two simultaneous recordings P1 and P2 showed dramatic differences regarding the amplitude of the first AP (Fig. 9B, upper trace, dashed line), in spite of careful series resistance and

capacitance compensation (Fig. 9B, lower trace). Membrane potential transients with slower dynamics, on the other hand, were not affected by a high-resistance pipette (Fig. 9AB, slow component). To address the impact of whole-cell capacitance on the amplitude of APs, we systematically increased whole-cell capacitance compensation of high resistance pipette P2 in equal steps of 1 pF (Methods). With each 1 pF step increase (Fig. 9C, Fig. 1–Fig. 9) the match between P2 and P1 AP amplitude and waveform improved. However, at one point, usually around 9 pF, the unwanted oscillations in the amplifier circuit disrupted the recordings (ringing) and the cells were lost. Our recording setup (Methods) invariably failed to obtain a good match between high resistance (P2) and low resistance (P1) records of the first AP. In Fig. 9D we plot only the best recording sweep obtained from each cell (n=13) just before the harmful oscillation destroyed the cell. More specifically, we plot the amplitude ratios P2/P1 for the first AP (9D, diamonds), as well as P2/P1 ratios for slow membrane potential changes (9D, circles), against the electrode resistance P2. We found that high resistance pipettes (36 – 58 MΩ) reduce the amplitudes of sodium APs by ~ 25% (average P2/P1 ratio = 75.2 ± 6.2%, range 67 – 85 %; n=8; Fig. 9D – eight diamonds on the right were averaged), without having any effect on the slow component (circles).

Due to a poor visibility of submicron structures in the brain slice preparation, patch clamp recordings from thin basal branches require near-infrared video microscopy combined with 2-photon fluorescence overlay (Nevian *et al.*, 2007). Formation of the gigaohm seal is accomplished by pulling a patch of dendritic membrane inside the mouth of the glass pipette. This mechanical manipulation carries a high risk for damaging the tiny dendritic branch; less than 1 μm in diameter. Our somatic whole-cell recordings, on the other hand, were performed under very favorable patching conditions. We dealt with the neuronal cell bodies, >15 μm in diameter. Neuronal cell bodies are easily visualized under ordinary Nomarski optics. Unlike the middle regions of basal dendrites (140 μm away from the soma), which are covered with densely packed numerous dendritic spine heads (Benavides-Piccione *et al.*, 2006), the neuronal somata have smooth and accessible membranes. Because the cell body is a smoother, larger and stronger structure than a thin basal dendrite, the robustness of the somatic patch-clamp recordings is greater than that of dendritic patch-clamp measurements. Nevertheless, in spite favorable patching conditions, when applied on the pyramidal cell body, high-resistance patch-pipettes still produce significant distortions in AP amplitude (Fig. 9B–D). These data suggest that high-resistance pipettes tend to underestimate the amplitude of the fast sodium action potential. On the other hand, “high-resistance” patch clamp recording is an accurate tool for addressing the soma-dendrite amplitude transfer function of slow voltage transients, such as synaptically-evoked plateau potentials or long hyperpolarizing pulses (Nevian *et al.*, 2007), because slow signals are not significantly distorted by high-resistance pipettes (Fig. 9D, circles). According to our measurements (Fig. 9D), patch clamp recordings performed with glass pipettes with electrode resistance ≤ 15 MΩ report accurate amplitudes of all electrical transients including the fast sodium action potential (Stuart *et al.*, 1997; Gasparini *et al.*, 2004).

Above we listed several possible technical reasons for the discrepancy between our data and conclusions of two recent studies (Kampa & Stuart, 2006; Nevian *et al.*, 2007). Another possible explanation for this discrepancy is the physiological difference between two cortical areas. The prefrontal cortex has several anatomical features, including dendritic spine density, distribution of dendrites and axons (Elston, 2003), and synaptic connectivity (Kritzer & Goldman-Rakic, 1995), which separates it from other cortical areas. It is plausible that one of the specializations of L5 pyramidal neurons in the prefrontal cortex is a stronger backpropagation of APs than that observed in the somatosensory cortex. A more likely explanation for discrepancy between our results and the Kampa and Stuart (2006) paper, is that our recordings were obtained in short and medium range basal dendrites. Our data did not eliminate the possibility that in the most distal segments of very long basal dendrites, changes

in AP amplitude and AP half-width may occur. According to recent voltage-imaging data (Kampa & Stuart, 2006), both the decline in AP amplitude and the significant broadening of a b-AP are taking place in the most remote segments of long dendritic branches, which are currently beyond our reach. It is important to limit the conclusions about basal dendrites of PFC pyramidal neurons to the segments measured (<245 μm from the soma), because basal dendrites from 3- to 5-week-old animals sometimes extend >300 μm from their soma (Fig. 10, Bottom row).

It must also be stated, that our data do not suggest that APs propagate with no attenuation into the basal dendritic tree. On the contrary, the amplitude of an AP decreases along the dendrite, which is reflected in the increase in AP half-width (Fig. 3) and decrease in AP-associated Ca^{2+} signal with distance from soma (Fig. 8); see also (Milojkovic *et al.*, 2007), their Fig. 3. Basal dendrites of cortical layer 5 pyramidal neurons, just like apical dendrites of the same cell type, are weakly excitable structures (Rapp *et al.*, 1996;Rhodes, 1999;Vetter *et al.*, 2001;Migliore & Shepherd, 2002). Basal dendrites show a very limited capability for generation of local sodium spikes. Only a small fraction (~12 %) of basal dendrites exposed to strong glutamatergic stimulation was able to produce a fast sodium spikelet (Milojkovic *et al.*, 2005b), thus suggesting that the ratio between sodium and potassium conductance in basal dendrites is significantly lower than in the cell body. Our present data indicate that in the prefrontal cortex APs backpropagate into distal tips of short basal dendrites with moderate amplitude and shape modulation, as previously shown for basal dendrites in the rat somatosensory cortex (Antic, 2003). Any studies dealing with the interaction of APs and synaptic contacts distributed in the proximal 150 μm from the soma (Fig. 10, dashed circles), should take into account that APs arrive in these regions in less than 1 ms (Fig. 3D), and look very similar to the somatic APs (Fig. 2 and Fig. 3B). These two features, together with an apparent lack of high-frequency amplitude boosting (Fig. 6), rule out a severe decline in AP amplitudes (down to 25% of its somatic amplitude) in this part of the basilar dendritic tree. Does this part of the basilar dendritic tree (proximal 150 μm) have any significant impact on the neuronal computational task? Judging from the spine density measurements, this portion of the basilar dendritic tree (proximal 150 μm), hosts a substantial fraction of synaptic contacts impinging on the PFC pyramidal cell. For example, in the rodent neocortex, the spine density profile along basal dendrite shows a gradual increase in the proximal 30 μm, a plateau between 50 and 90 μm, and gradual decline beyond 100 μm from the soma (Benavides-Piccione *et al.*, 2006)(their figure 3B). Based on the spine density studies the proximal 150 μm of basal segments receive a significant fraction of the total excitatory synaptic drive.

In the sample of 21 pyramidal neurons filled with fluorescent dyes (Fig. 10) we measured the fraction of the total basilar dendritic membrane contained in the first 150 μm from the soma (dashed circles). We found that the proximal 150 μm of basilar dendritic branches comprise 81.1 ± 8.4% of the total length of the basilar dendritic tree in the rat medial prefrontal cortex (Fig. 10, pie chart). Wang et al., (2006) made Neurolucida reconstructions of biocytine-filled pyramidal neurons in the ferret prefrontal cortex. In their representative example (their figure 1) all putative synaptic contacts between two neighboring layer 5 pyramidal neurons (8 out of 8) were detected within 150 μm from the cell body (Wang *et al.*, 2006), see also (Markram *et al.*, 1997) their Fig. 1A. For these reasons it would be incorrect to assume that AP failure model (Kampa & Stuart, 2006) generally and indiscriminately applies to all basal dendrites and to all segments of the basilar dendritic tree. On the contrary, a significant fraction of synaptic contacts in the basilar dendritic tree of prefrontal cortical layer 5 pyramidal neurons experience fast and substantial voltage transients during somatic firing.

Long versus short basal branches

One intriguing result of the present study is an apparent dichotomy of AP backpropagation in the basilar dendritic tree of cortical pyramidal neurons. The basilar dendritic tree is composed of dendrites with variable lengths and variable number of branch points (Fig. 10). While longer branches impose a great deal of attenuation and filtering (Kampa & Stuart, 2006), shorter dendrites impose significantly lesser degree of attenuation on backpropagating APs (Fig. 1–Fig. 8). As a result, a qualitatively and quantitatively different electrical signal occurs in dendritic tips of long and short branches during the same action potential event (Fig. 2, compare B – F). This may cause synaptic contacts in dendritic tips of short and long basal dendrites to employ different rules of spike timing-dependent synaptic plasticity (Gordon *et al.*, 2006;Letzkus *et al.*, 2006;Sjostrom & Hausser, 2006). Besides dendritic geometry (diameter, length, and branch points) it is important to consider in the future whether non-uniform distribution of dendritic voltage-gated conductances may also cause the dichotomy of AP backpropagation (Golding *et al.*, 2001). In any case, the present (Fig. 2) and recent (Milojkovic *et al*., 2005b;Gasparini *et al*., 2007) physiological data suggest that the same class of dendritic branches (e.g. basal, oblique) belonging to one pyramidal neuron may exhibit different electrical transients during the same AP event.

Supplementary Material

Refer to Web version on PubMed Central for supplementary material.

Acknowledgements

We are grateful to Andrew Millard for laser-to-microscope optical coupling, to Corey Acker and Matt Wachowiak for writing the software used in data analysis, and to Corey Acker for comments on the manuscript. Supported by NIH grants MH63035 and EB001963.

Abbreviations

ACSF, Artificial cerebrospinal fluid; AP, Action potential; b-AP, Backpropagating AP; CG-1, Calcium Green – 1; NMDA, N-methyl-D-aspartate; PFC, Prefrontal cortex; VSD, Voltage-sensitive dye.

References

Antic S, Major G, Zecevic D. Fast optical recordings of membrane potential changes from dendrites of pyramidal neurons. J Neurophysiol 1999;82:1615–1621. [PubMed: 10482775]

Antic SD. Action potentials in basal and oblique dendrites of rat neocortical pyramidal neurons. J Physiol 2003;550:35–50. [PubMed: 12730348]

Araya R, Eisenthal KB, Yuste R. Dendritic spines linearize the summation of excitatory potentials. Proc Natl Acad Sci U S A 2006;103:18799–18804. [PubMed: 17132736]

Benavides-Piccione R, Hamzei-Sichani F, Ballesteros-Yanez I, DeFelipe J, Yuste R. Dendritic size of pyramidal neurons differs among mouse cortical regions. Cereb Cortex 2006;16:990–1001. [PubMed: 16195469]

Burkhalter A. Intrinsic connections of rat primary visual cortex: laminar organization of axonal projections. J Comp Neurol 1989;279:171–186. [PubMed: 2913064]

Chafee MV, Goldman-Rakic PS. Matching patterns of activity in primate prefrontal area 8a and parietal area 7ip neurons during a spatial working memory task. J Neurophysiol 1998;79:2919–2940. [PubMed: 9636098]

Chang JY, Janak PH, Woodward DJ. Neuronal and behavioral correlations in the medial prefrontal cortex and nucleus accumbens during cocaine self-administration by rats. Neuroscience 2000;99:433–443. [PubMed: 11029536]

Dan Y, Poo MM. Spike timing-dependent plasticity of neural circuits. Neuron 2004;44:23–30. [PubMed: 15450157]

Elston GN. Cortex, cognition and the cell: New insights into the pyramidal neuron and prefrontal function. Cereb Cortex 2003;13:1124–1138. [PubMed: 14576205]

Elston GN, Benavides-Piccione R, DeFelipe J. The pyramidal cell in cognition: a comparative study in human and monkey. J Neurosci 2001;21:RC163. [PubMed: 11511694]

Enoki R, Kiuchi T, Koizumi A, Sasaki G, Kudo Y, Miyakawa H. NMDA receptor-mediated depolarizing after-potentials in the basal dendrites of CA1 pyramidal neurons. Neurosci Res 2004;48:325–333. [PubMed: 15154678]

Feldmeyer D, Lubke J, Silver RA, Sakmann B. Synaptic connections between layer 4 spiny neurone-layer 2/3 pyramidal cell pairs in juvenile rat barrel cortex: physiology and anatomy of interlaminar signalling within a cortical column. J Physiol 2002;538:803–822. [PubMed: 11826166]

Gasparini S, Losonczy A, Chen X, Johnston D, Magee JC. Associative pairing enhances action potential back-propagation in radial oblique branches of CA1 pyramidal neurons. J Physiol 2007;580:289–302.

Gasparini S, Migliore M, Magee JC. On the initiation and propagation of dendritic spikes in CA1 pyramidal neurons. J Neurosci 2004;24:11046–11056. [PubMed: 15590921]

Golding NL, Kath WL, Spruston N. Dichotomy of action-potential backpropagation in CA1 pyramidal neuron dendrites. J Neurophysiol 2001;86:2998–3010. [PubMed: 11731556]

Goldman-Rakic PS. Cellular basis of working memory. Neuron 1995;14:477–485. [PubMed: 7695894]

Gordon U, Polsky A, Schiller J. Plasticity compartments in basal dendrites of neocortical pyramidal neurons. J Neurosci 2006;26:12717–12726. [PubMed: 17151275]

Gulledge AT, Jaffe DB. Dopamine decreases the excitability of layer V pyramidal cells in the rat prefrontal cortex. J Neurosci 1998;18:9139–9151. [PubMed: 9787016]

Holthoff K, Kovalchuk Y, Konnerth A. Dendritic spikes and activity-dependent synaptic plasticity. Cell Tissue Res 2006;326:369–377. [PubMed: 16816965]

Homayoun H, Moghaddam B. Bursting of prefrontal cortex neurons in awake rats is regulated by metabotropic glutamate 5 (mGlu5) receptors: rate-dependent influence and interaction with NMDA receptors. Cereb Cortex 2006;16:93–105. [PubMed: 15843630]

Jaffe DB, Johnston D, Lasser-Ross N, Lisman JE, Miyakawa H, Ross WN. The spread of Na+ spikes determines the pattern of dendritic Ca2+ entry into hippocampal neurons. Nature 1992;357:244–246. [PubMed: 1350327]

Kampa BM, Letzkus JJ, Stuart GJ. Requirement of dendritic calcium spikes for induction of spike-timing-dependent synaptic plasticity. J Physiol 2006;574:283–290. [PubMed: 16675489]

Kampa BM, Stuart GJ. Calcium spikes in basal dendrites of layer 5 pyramidal neurons during action potential bursts. J Neurosci 2006;26:7424–7432. [PubMed: 16837590]

Koester HJ, Sakmann B. Calcium dynamics in single spines during coincident pre-and postsynaptic activity depend on relative timing of back-propagating action potentials and subthreshold excitatory postsynaptic potentials. Proc Natl Acad Sci USA 1998;95:9596–9601. [PubMed: 9689126]

Kritzer MF, Goldman-Rakic PS. Intrinsic circuit organization of the major layers and sublayers of the dorsolateral prefrontal cortex in the rhesus monkey. J Comp Neurol 1995;359:131–143. [PubMed: 8557842]

Larkman AU. Dendritic morphology of pyramidal neurones of the visual cortex of the rat: III. Spine distributions. J Comp Neurol 1991;306:332–343. [PubMed: 1711059]

Larkum ME, Zhu JJ, Sakmann B. Dendritic mechanisms underlying the coupling of the dendritic with the axonal action potential initiation zone of adult rat layer 5 pyramidal neurons. J Physiol (Lond) 2001;533:447–466. [PubMed: 11389204]

Letzkus JJ, Kampa BM, Stuart GJ. Learning rules for spike timing-dependent plasticity depend on dendritic synapse location. J Neurosci 2006;26:10420–10429. [PubMed: 17035526]

Levitt JB, Lewis DA, Yoshioka T, Lund JS. Topography of pyramidal neuron intrinsic connections in macaque monkey prefrontal cortex (areas 9 and 46). J Comp Neurol 1993;338:360–376. [PubMed: 8113445]

Linden DJ. The return of the spike: postsynaptic action potentials and the induction of LTP and LTD. Neuron 1999;22:661–666. [PubMed: 10230787]

Lisman J, Malenka RC, Nicoll RA, Malinow R. Learning mechanisms: the case for CaM-KII. Science 1997;276:2001–2002. [PubMed: 9221509]

London M, Schreibman A, Hausser M, Larkum ME, Segev I. The information efficacy of a synapse. Nat Neurosci 2002;5:332–340. [PubMed: 11896396]

Lubke J, Roth A, Feldmeyer D, Sakmann B. Morphometric analysis of the columnar innervation domain of neurons connecting layer 4 and layer 2/3 of juvenile rat barrel cortex. Cereb Cortex 2003;13:1051–1063. [PubMed: 12967922]

Magee JC, Johnston D. A synaptically controlled, associative signal for Hebbian plasticity in hippocampal neurons. Science 1997;275:209–213. [PubMed: 8985013]

Markram H. A network of tufted layer 5 pyramidal neurons. Cereb Cortex 1997;7:523–533. [PubMed: 9276177]

Markram H, Lubke J, Frotscher M, Sakmann B. Regulation of synaptic efficacy by coincidence of postsynaptic APs and EPSPs. Science 1997;275:213–215. [PubMed: 8985014]

Migliore M, Shepherd GM. Emerging rules for the distributions of active dendritic conductances. Nat Rev Neurosci 2002;3:362–370. [PubMed: 11988775]

Milojkovic BA, Radojicic MS, Antic SD. A strict correlation between dendritic and somatic plateau depolarizations in the rat prefrontal cortex pyramidal neurons. J Neurosci 2005a;25:3940–3951. [PubMed: 15829646]

Milojkovic BA, Wuskell JP, Loew LM, Antic SD. Initiation of sodium spikelets in basal dendrites of neocortical pyramidal neurons. J Membr Biol 2005b;208:155–169. [PubMed: 16645744]

Milojkovic BA, Zhou WL, Antic SD. Voltage and Calcium Transients in Basal Dendrites of the Rat Prefrontal Cortex. J Physiol 2007;585:447–468. [PubMed: 17932150]

Morishima M, Kawaguchi Y. Recurrent connection patterns of corticostriatal pyramidal cells in frontal cortex. J Neurosci 2006;26:4394–4405. [PubMed: 16624959]

Nevian T, Larkum ME, Polsky A, Schiller J. Properties of basal dendrites of layer 5 pyramidal neurons: a direct patch-clamp recording study. Nat Neurosci 2007;10:206–214. [PubMed: 17206140]

Nevian T, Sakmann B. Spine Ca2+ signaling in spike-timing-dependent plasticity. J Neurosci 2006;26:11001–11013. [PubMed: 17065442]

Oakley JC, Schwindt PC, Crill WE. Dendritic calcium spikes in layer 5 pyramidal neurons amplify and limit transmission of ligand-gated dendritic current to soma. J Neurophysiol 2001;86:514–527. [PubMed: 11431529]

Polsky A, Mel BW, Schiller J. Computational subunits in thin dendrites of pyramidal cells. Nat Neurosci 2004;7:621–627. [PubMed: 15156147]

Ramus SJ, Eichenbaum H. Neural correlates of olfactory recognition memory in the rat orbitofrontal cortex. J Neurosci 2000;20:8199–8208. [PubMed: 11050143]

Rapp M, Yarom Y, Segev I. Modeling back propagating action potential in weakly excitable dendrites of neocortical pyramidal cells. Proc Natl Acad Sci USA 1996;93:11985–11990. [PubMed: 8876249]

Rhodes, PA. Functional implications of active currents in the dendrites of pyramidal neuros. In: Ulinski, PJ.; E, G., editors. Cerebral cortex. New York: Kluwer Academic/ Plenum Publishers; 1999. p. 139-200.

Ross WN, Salzberg BM, Cohen LB, Grinvald A, Davila HV, Waggoner AS, Wang CH. Changes in absorption, fluorescence, dichroism, and Birefringence in stained giant axons: : optical measurement of membrane potential. J Membr Biol 1977;33:141–183. [PubMed: 864685]

Schiller J, Major G, Koester HJ, Schiller Y. NMDA spikes in basal dendrites of cortical pyramidal neurons. Nature 2000;404:285–289. [PubMed: 10749211]

Sjostrom PJ, Hausser M. A cooperative switch determines the sign of synaptic plasticity in distal dendrites of neocortical pyramidal neurons. Neuron 2006;51:227–238. [PubMed: 16846857]

Spruston N, Schiller Y, Stuart G, Sakmann B. Activity-dependent action potential invasion and calcium influx into hippocampal CA1 dendrites. Science 1995;268:297–300. [PubMed: 7716524]

Staiger JF, Kotter R, Zilles K, Luhmann HJ. Laminar characteristics of functional connectivity in rat barrel cortex revealed by stimulation with caged-glutamate. Neurosci Res 2000;37:49–58. [PubMed: 10802343]

Stuart G, Schiller J, Sakmann B. Action potential initiation and propagation in rat neocortical pyramidal neurons. J Physiol (Lond) 1997;505:617–632. [PubMed: 9457640]

Thomson AM, Bannister AP. Interlaminar connections in the neocortex. Cereb Cortex 2003;13:5–14. [PubMed: 12466210]

Vetter P, Roth A, Hausser M. Propagation of action potentials in dendrites depends on dendritic morphology. J Neurophysiol 2001;85:926–937. [PubMed: 11160523]

Wang Y, Markram H, Goodman PH, Berger TK, Ma J, Goldman-Rakic PS. Heterogeneity in the pyramidal network of the medial prefrontal cortex. Nat Neurosci 2006;9:534–542. [PubMed: 16547512]

Williams GV, Goldman-Rakic PS. Modulation of memory fields by dopamine D1 receptors in prefrontal cortex. Nature 1995;376:572–575. [PubMed: 7637804]

Zhou WL, Yan P, Wuskell JP, Loew LM, Antic SD. Intracellular long wavelength voltage-sensitive dyes for studying the dynamics of action potentials in axons and thin dendrites. J Neurosci Meth 2007;164:225–239.

Zucker RS. Calcium- and activity-dependent synaptic plasticity. Curr Opin Neurobiol 1999;9:305–313. [PubMed: 10395573]

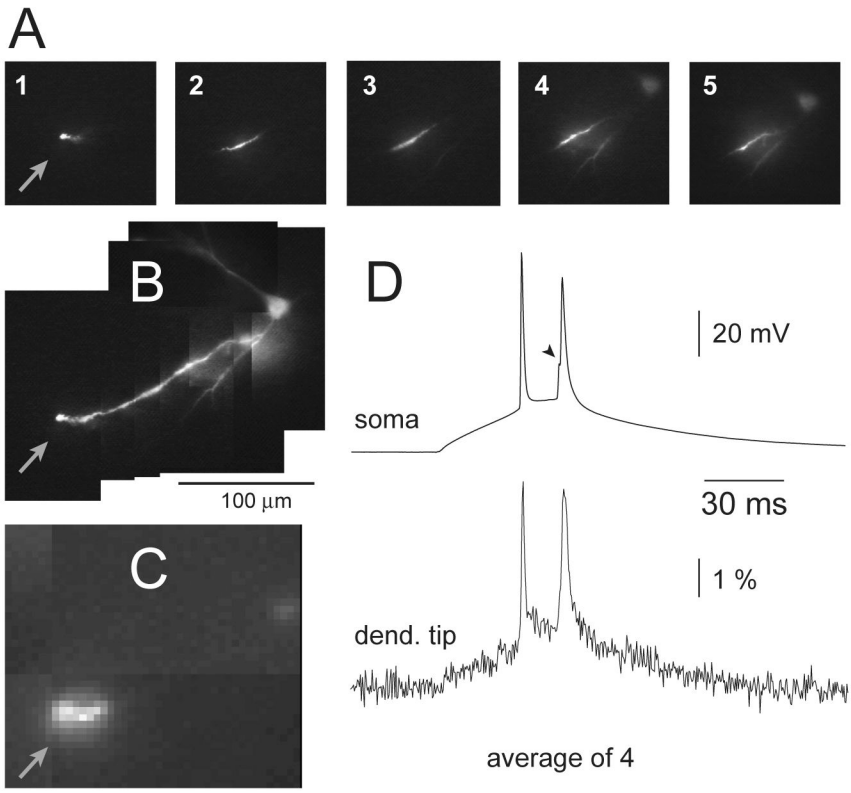

Fig. 1.

Laser spot illumination. (**A**) Five images (1–5) of different dendritic segments illuminated by a motionless laser spot (~50 µm in diameter). (**B**) A composite image made from images 1–5 shown in **A**. (**C**) Blow up of image 1. Arrow marks the very end of the dendritic branch (dendritic tip). (**D**) Simultaneous somatic (whole-cell) and dendritic (VSD) recordings of an AP doublet. VSD trace is product of 4 sweeps (temporal averaging) and 8 neighboring pixels (spatial averaging) filtered with low-pass Gaussian 1050 Hz cut-off. The first AP was used for spike-triggered averaging (n=4). Arrowhead marks the glitch on the rising phase of the second AP caused by the AP trial-to-trial jitter (inconsistent time interval between 1st and 2nd AP). For the same reason, dendritic 2nd AP is also distorted in the temporal domain.

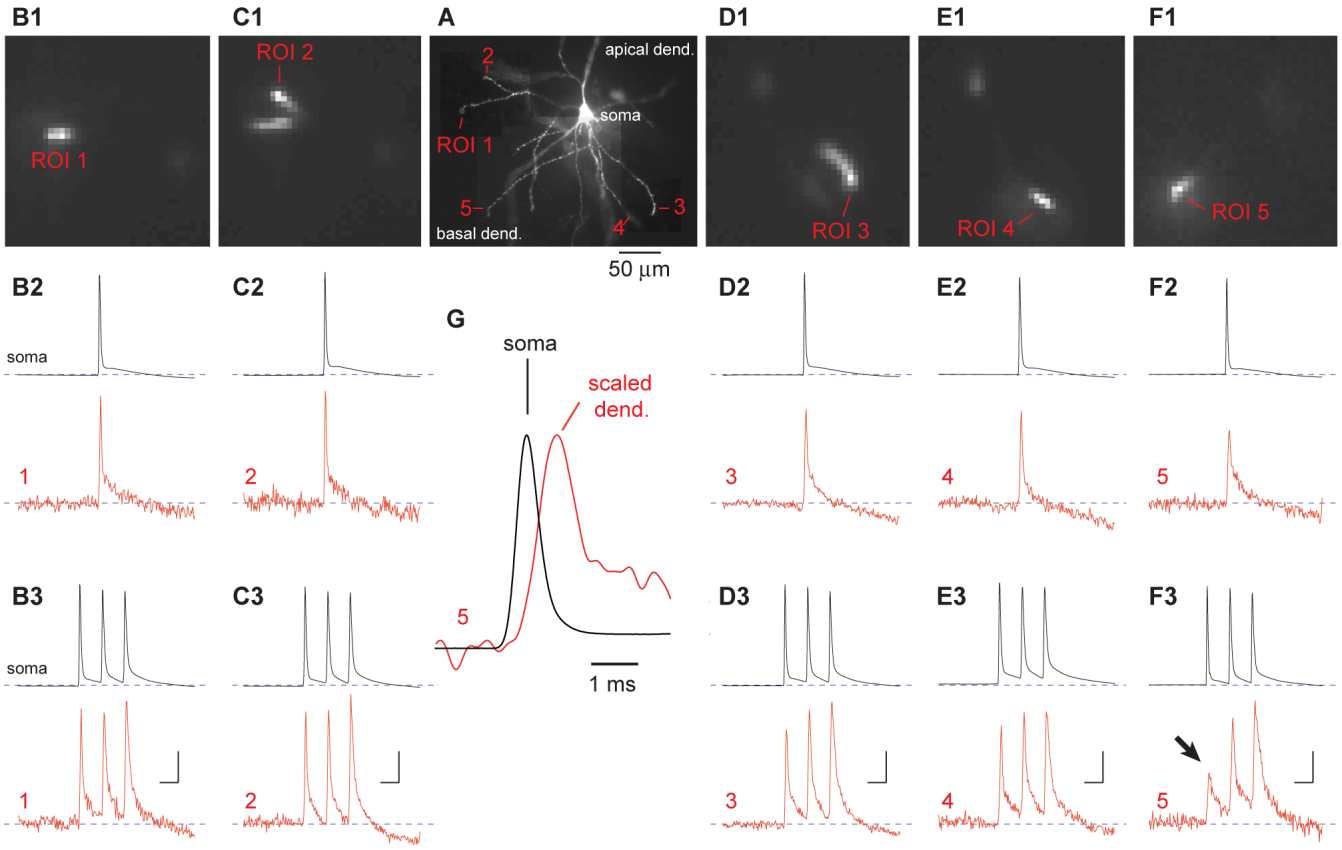

Fig. 2.

Voltage-sensitive dye (VSD) recordings from tips of basal dendrites. (**A**) Microphotograph of a neuron filled with JPW3028. (**B1-F1**) One frame acquired during voltage imaging from the region of interest as indicated in A. (**B2-F2**) Simultaneous recording of a single AP from the soma (whole-cell) and dendritic tip (voltage imaging, ROIs 1–5). (**B3-F3**) Same as in **B2-F2** except the neuron was stimulated to produce a triplet of AP at 80 Hz. Arrow marks an AP that failed to invade the dendritic tip. Scale bars 10 ms and 2 % ΔF/F. (G) Somatic AP is superimposed with dendritic signal from ROI 5 to show the difference in duration (half-width). Two signals are filtered with Gaussian low-pass 800 Hz cutoff, interpolated and scaled to the same height.

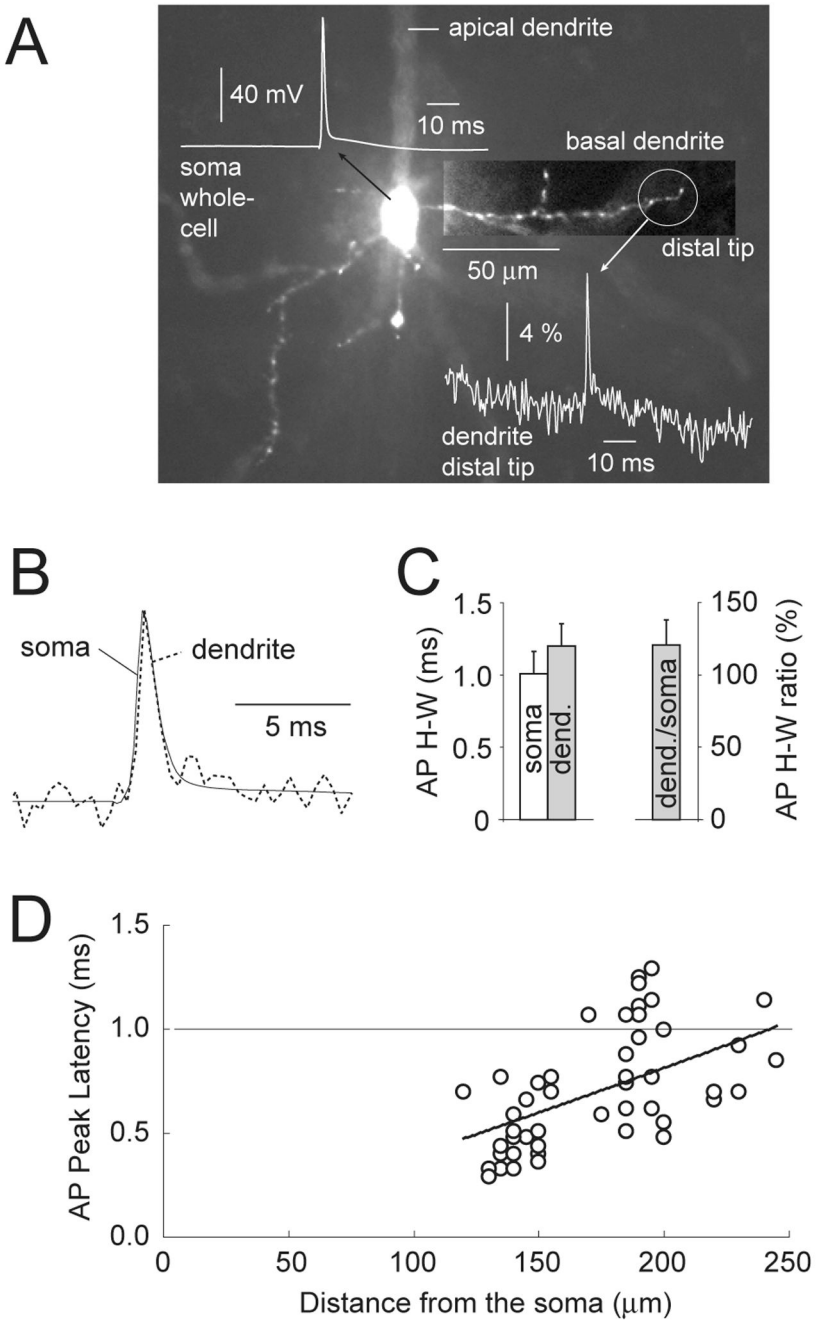

Fig. 3.

AP half-width in the distal dendritic tip. (**A**) Composite microphotograph of a L5 pyramidal neuron filled with JPW4090. Basal dendrite of interest is shown with enhanced contrast. Simultaneous somatic (soma whole-cell) and VSD dendritic (dendrite distal tip) recordings are pasted onto the image. (**B**) The same two recordings are superimposed to show the similarity in AP half-width obtained at two recording sites. (**C**) An average AP half-width at soma and distal dendrite (Left) and dendrite/soma ratio (Right) are presented in the form of a bar diagram (n=46 distal dendritic tips obtained in 21 pyramidal neurons). (**D**) AP peak latency measured in the distal tip is plotted against the distance between the distal tip and the soma (n=same as in **C**).

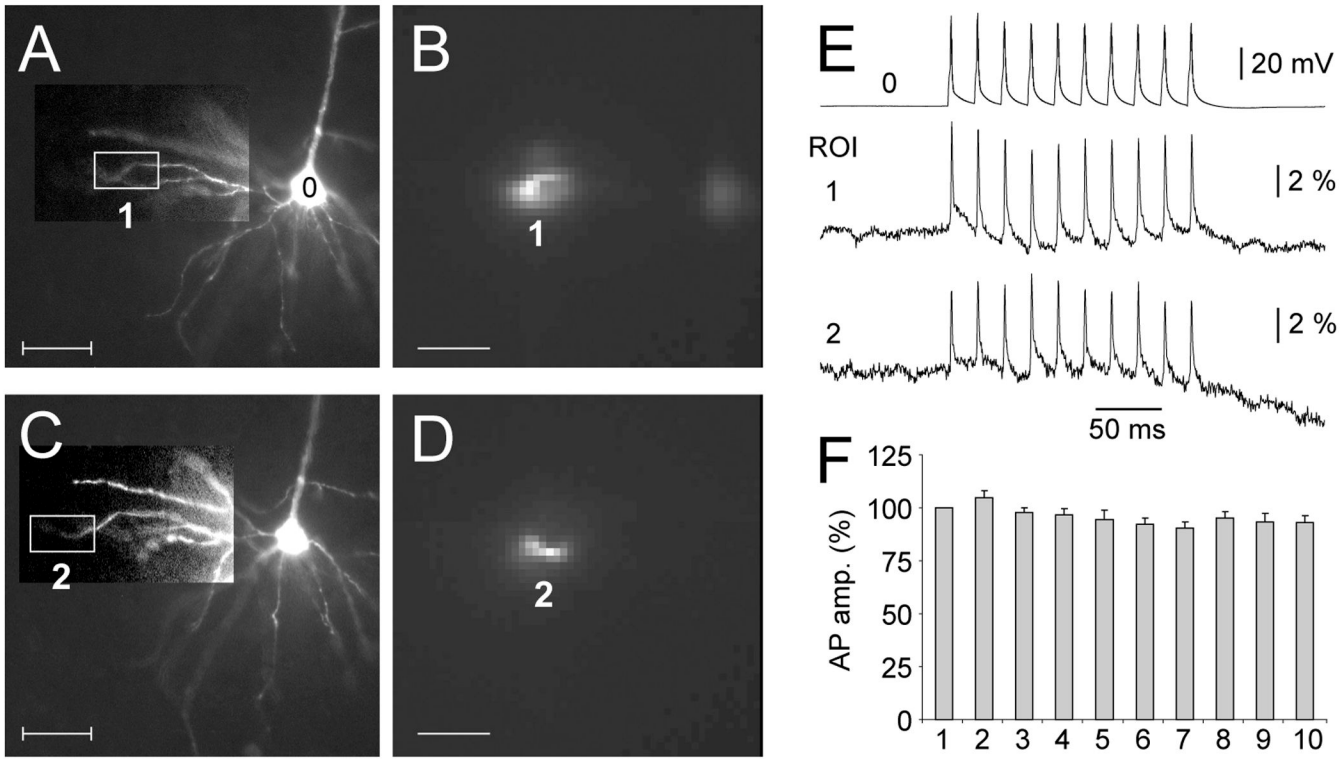

Fig. 4.

Trains of APs backpropagate into basal dendrites. (**A** and **C**) Microphotograph of the dendritic tree. Basal dendrite of interest is shown with enhanced contrast. (**B** and **D**) Laser spot is illuminating an area marked by boxes in **A** and **C**. Image was captured by fast data acquisition camera (80 × 80 pixels). (**E**) Simultaneous somatic whole-cell (0) and VSD dendritic recordings of 10 APs (50 Hz) obtained from two regions of interest (ROIs 1 and 2). Each optical signal is product of temporal (n=4 sweeps) and spatial averaging (n=6 pixels). (**F**) AP amplitudes of spikes 2 – 10 are expressed relative to the amplitude of the first AP in the train and averaged across 7 recording sites obtained in 3 neurons. Average distance of ROI from the soma was 127 ± 22 μm. Scale bars = 50 μm.

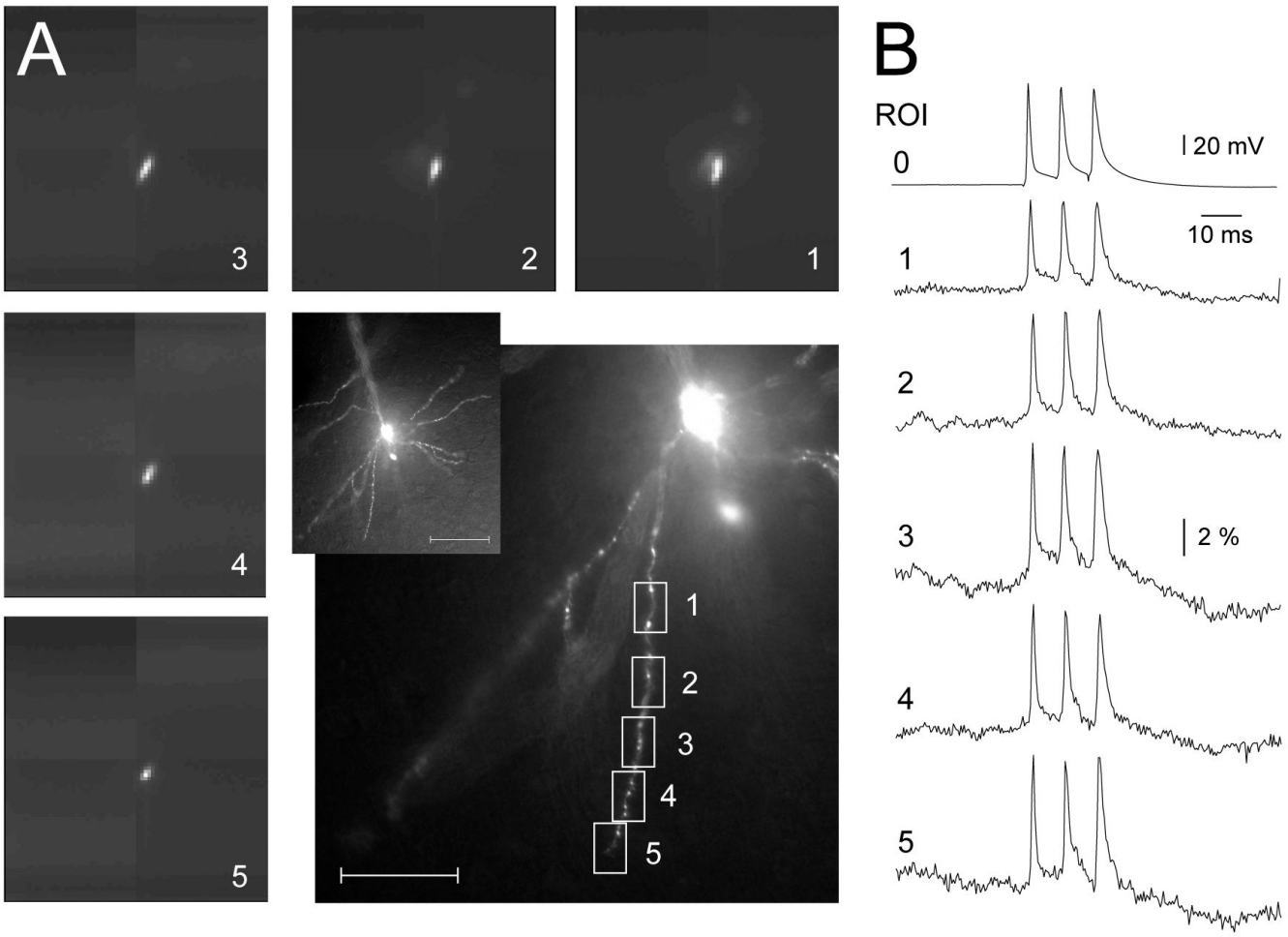

Fig. 5.

Sequential multi-site VSD recordings of backpropagating APs. (**A**) Five images on the outside rim (1–5) are products of laser spot illumination and fast data acquisition (80 × 80 pixel camera). Images 1–5 correspond to dendritic segments 1–5 marked by boxes in the central photograph. Central corner inset depicts the pyramidal cell under study. Scale bars are 50 μm (central image) and 100 μm (corner inset). (**B**) Simultaneous somatic whole-cell (ROI 0) and dendritic (ROI 1) recording. In the subsequent sweep simultaneous somatic (not shown) and dendritic (ROI 2) was sampled. The sequence was repeated until the last dendritic region was probed with VSD imaging. Each optical trace is product of temporal (n=4 sweeps) and spatial averaging (3–6 neighboring pixels).

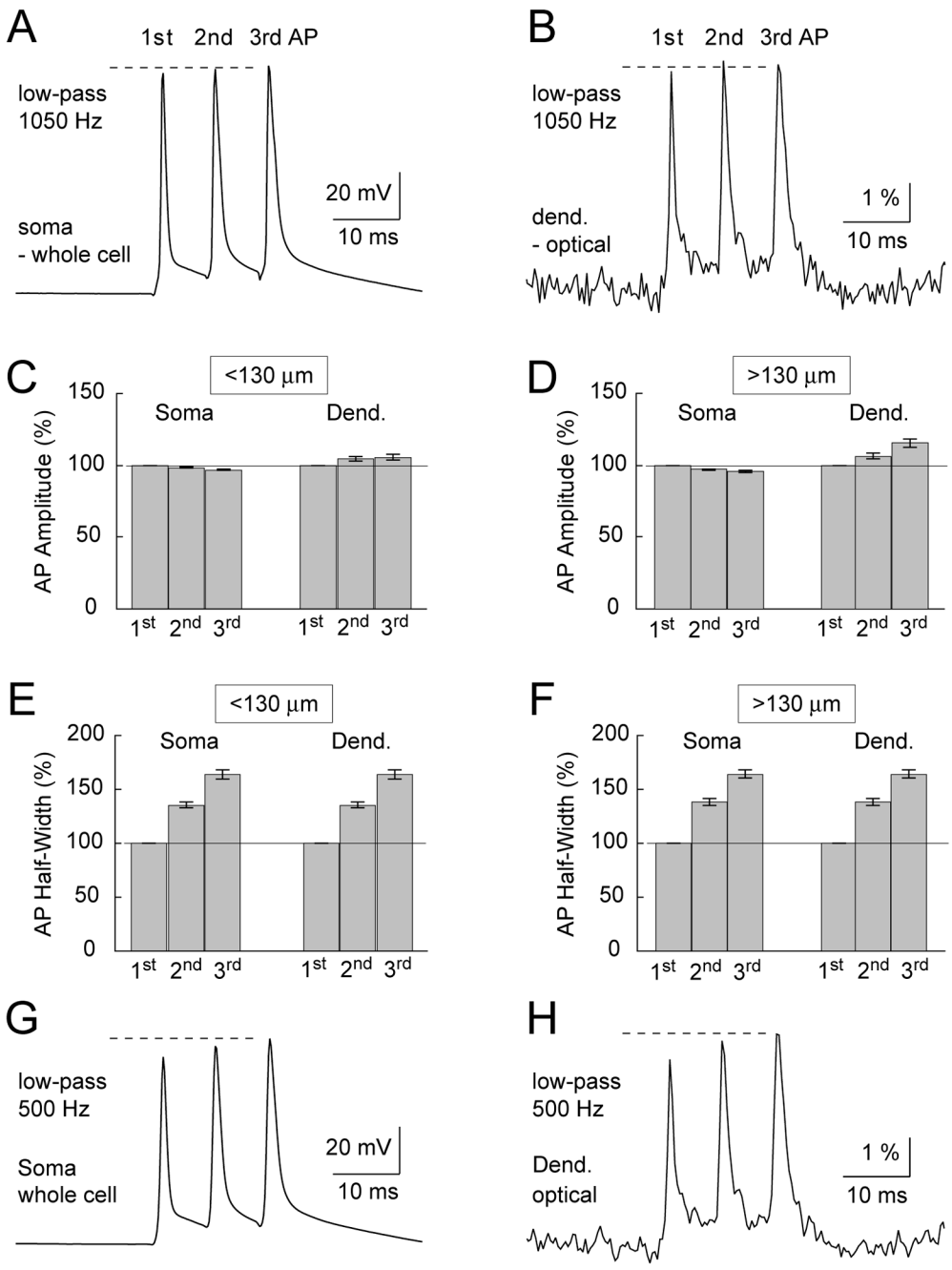

Fig. 6.

AP backpropagation during high frequency AP burst. (**A**) Somatic whole-cell recording of an AP triplet (125 Hz). (**B**) Dendritic VSD recording (of the same burst shown in **A**) obtained from the distal dendritic tip, 155 µm away from the soma. Data set is divided into two groups (**C** and **D**), based on the distance of the VSD dendritic recording site from the soma. (**C**) Dendritic recordings obtained less than 130 µm from the soma (Dend.) and their corresponding somatic whole-cell records (Soma). Amplitudes of the 2nd and 3rd AP in the triplet are normalized in respect to the first spike and averaged across neurons. (**D**) Same as in **C** except dendritic recordings were obtained at distances greater than 130 µm from the soma. (**E**) Half-widths of the 2nd and 3rd AP in the triplet are normalized in respect to the first spike and

averaged across neurons. (**F**) Same as in **E** except dendritic recordings were obtained at distances greater than 130 μm from the soma. (**G**) Whole-cell recording shown in **A** was passed through a low-pass digital filter 500 Hz cut-off. (**H**) Optical trace shown in **B** was passed through the same filter. Note that filtering at 500 Hz cut-off dramatically affects the 1st AP in both electrical and optical recordings.

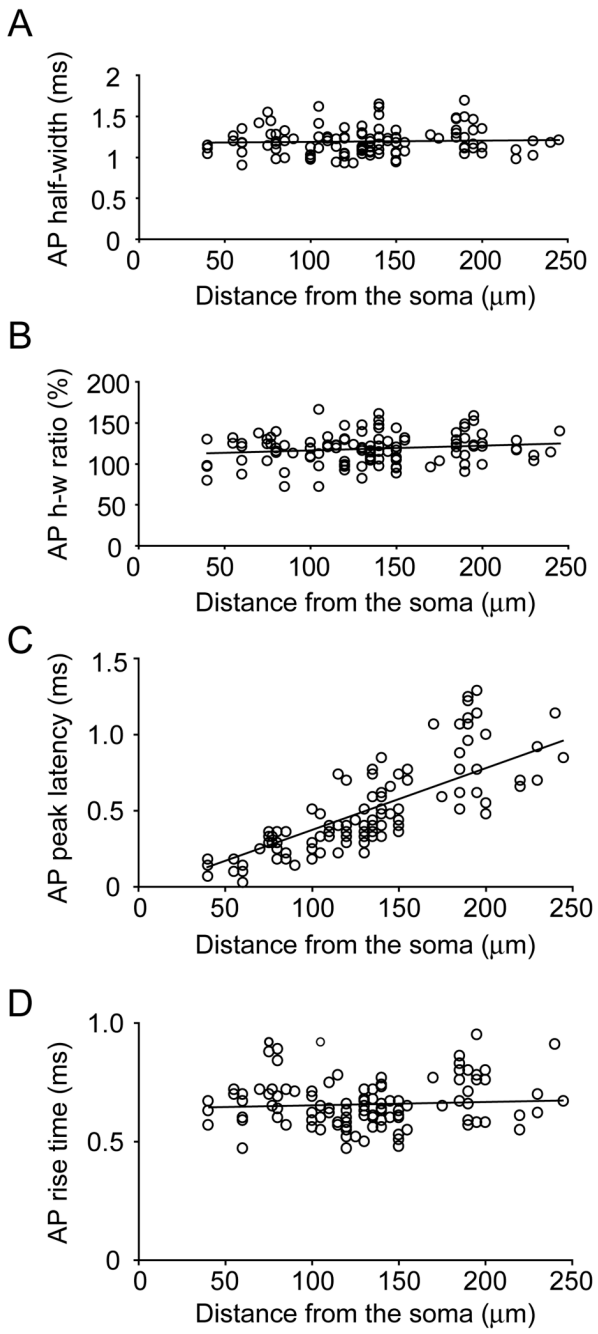

Fig. 7.

AP backpropagation in basal dendrites. Group data include data points sampled from distal dendritic tips (shown in Fig. 3) combined with those sampled from proximal (<150 um) dendritic regions of 39 pyramidal neurons in the rat prefrontal cortex. (**A**) Absolute AP duration (AP half-width) in milliseconds is plotted versus distance from the soma. (**B**) The same data as in **A** except AP half-width are normalized in respect to the AP half-width obtained in the somatic whole-cell record. (**C**) Time interval between the somatic and dendritic AP (peak latency) is plotted vs. distance. (**D**) AP rise time (from 10% amplitude to 90% amplitude) is plotted vs. distance.

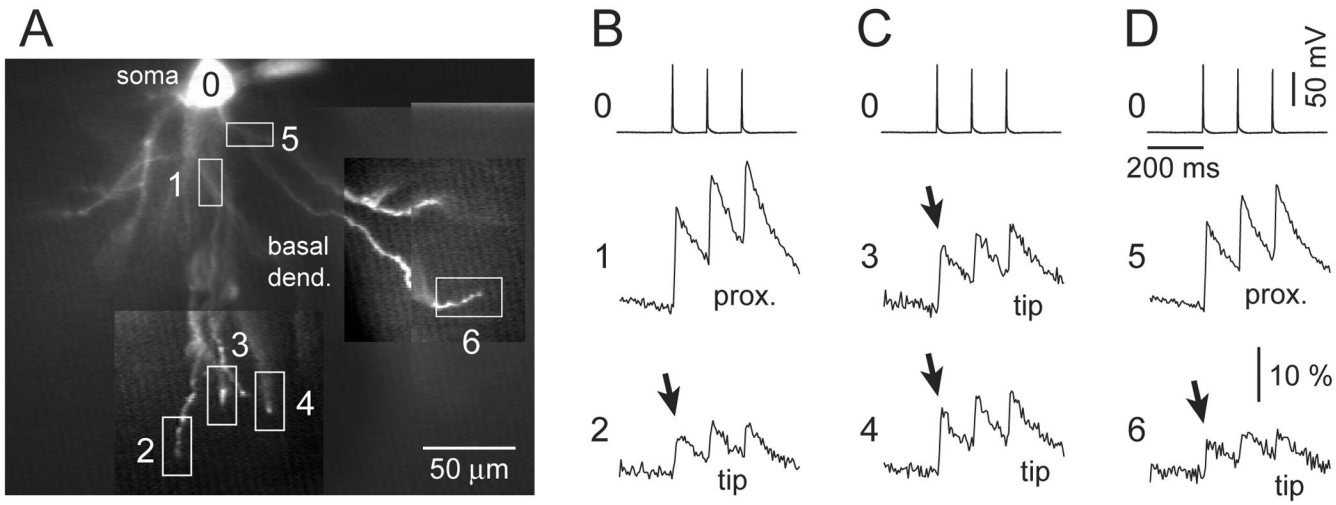

Fig. 8.

AP-associated Ca^{2+} transients in basal dendrites. (**A**) Microphotograph of a neuron filled with CG-1 and Alexa Fluor. Boxes mark regions of interest where optical signals were chosen for display in panels B–D. Triplets of APs (120 ms inter-spike interval) were evoked by three depolarizing pulses of current injected into the soma. (**B**) Calcium transient from the tip of the basal dendrite (ROI 2) is aligned with Ca^{2+} signal from the proximal dendritic segment (ROI 1) and the somatic whole-cell recording (0). (**C**) AP- associated Ca^{2+} transients from two dendritic tips (ROIs 3–4) as indicated in A. (**D**) Same as in **B** except different basal dendrite. Arrow marks a sharp Ca^{2+} transient associated with the first AP in the train.

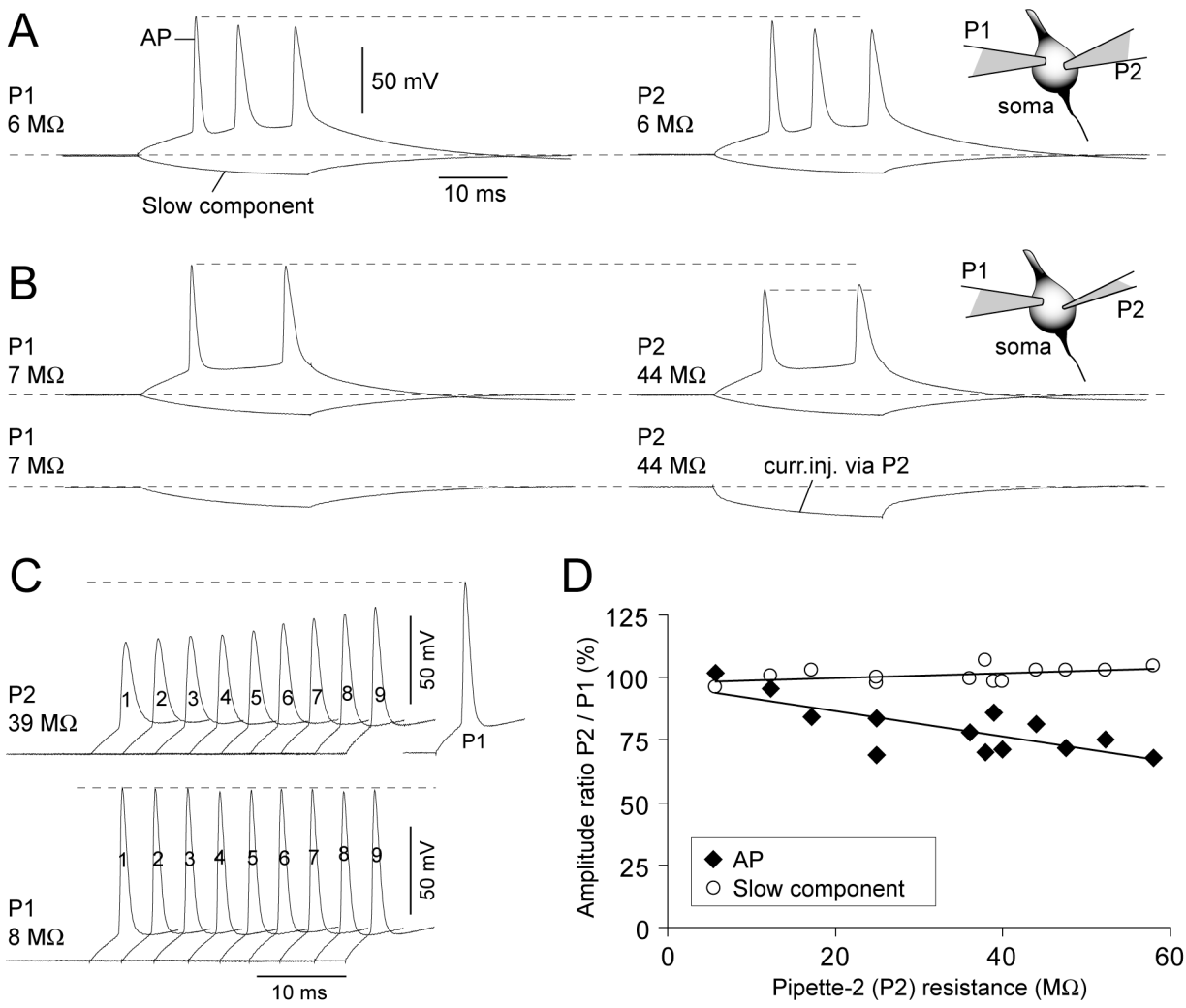

Fig. 9.

High resistance pipettes tend to underestimate the AP amplitude. (**A**) Inset: Schematic drawing of the experimental design. Cell bodies of pyramidal L5 neurons were patched with two pipettes. Both pipettes P1 and P2 are regular whole-cell pipettes of equal size (electrode resistance = 6 MΩ). Upper trace: The same triplet of action potentials recorded on two channels simultaneously. Dashed line indicates good match between AP amplitudes. Lower trace: Simultaneous dual patch recording of slow voltage signal evoked by a hyperpolarizing pulse injected via P1. (**B**) Inset: Pipette P1 has a low electrode resistance (7 MΩ). Pipette P2 has a high electrode resistance (44 MΩ). Upper trace: Although both pipettes record the same electrical event (AP doublet) from the same cell body, the AP amplitude on channel P2 is significantly smaller than that obtained through P1 (dashed lines). Slow signal (hyperpolarization pulse) is not affected. Lower traces: Current injections through P1 (left) and P2 (right) were used to adjust pipette capacitance and bridge balance. (**C**) The effect of pipette capacitance neutralization (1 – 9 pF) on the AP amplitude. After each step-increase in pipette capacitance, but before the actual recording (sweep 1 – 9), the bridge balance was re-adjusted. (**D**) AP peak amplitude recorded with P2 is divided by AP peak amplitude recorded with P1 pipette and plotted versus the P2 electrode resistance (diamonds). Circles represent P2/P1 amplitude ratio for slow component (measured at 23 ms from the onset of the current pulse).

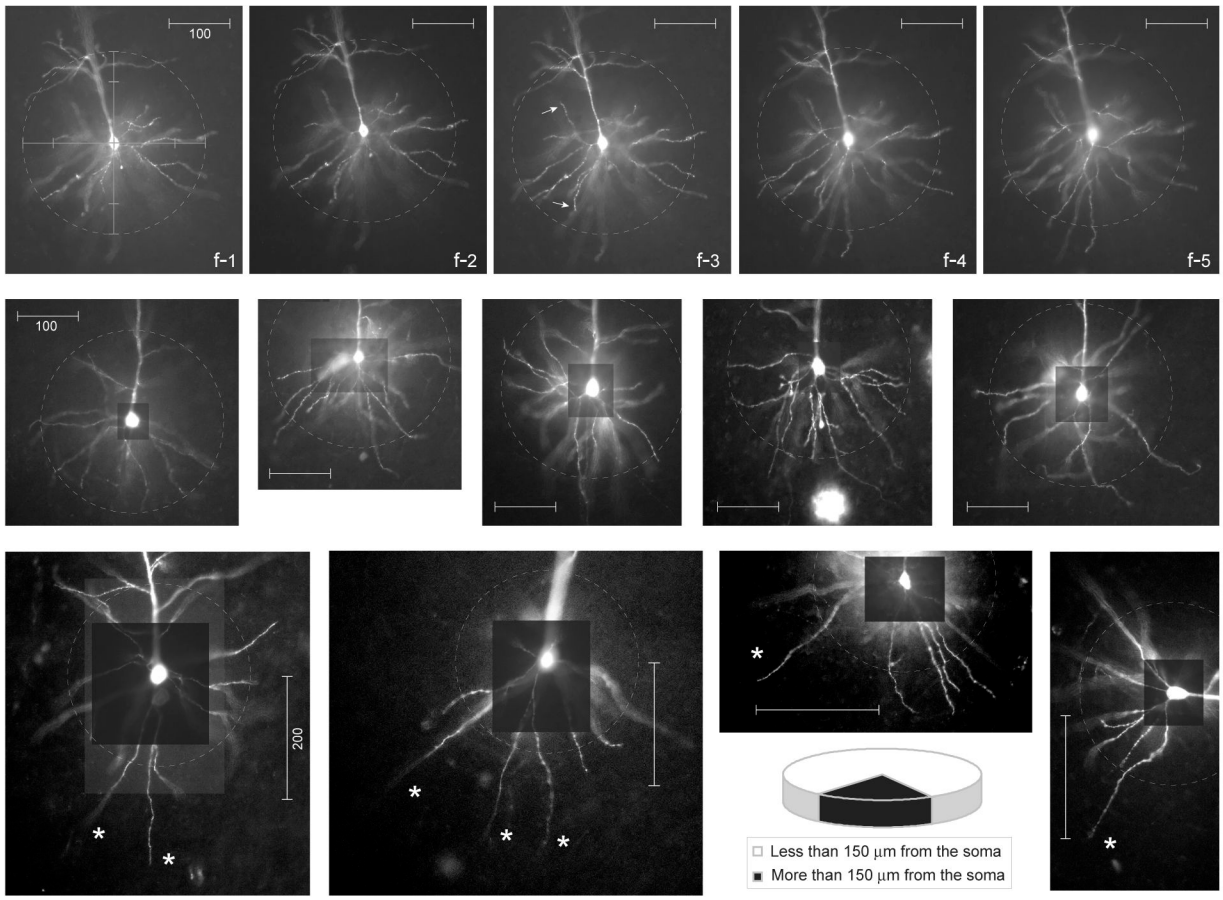

Fig. 10.

Geometry of basal dendrites in the rat medial prefrontal cortex. **Top row**: Fluorescent microphotograph of the basilar dendritic tree at 5 different focal planes (f1 – f5) used to trace individual dendritic branches from the soma to the distal tip. Scale bar = 100 μm. Dashed circle marks an area around the cell body, 150 μm in radius. Arrows mark terminal dendritic segments (dendritic tips) less than 150 μm path-distance from the soma. **Middle row**: Five typical layer 5 pyramidal neurons selected from the data set (n=21). Scale bar = 100 μm. **Bottom row**: Examples of layer 5 pyramidal cells with long basal dendrites. Scale bar = 200 μm. Asterisks mark terminal dendritic segments (dendritic tips) more than 300 μm path distance from the soma. The fractions of dendritic length inside (white) and outside (black) the 150 μm-perimeter are plotted in the pie chart.